

Interference between Coulomb and nuclear excitation in the inelastic scattering of ^{22}Ne from $^{88}\text{Sr}^\dagger$

E. E. Gross, H. G. Bingham, M. L. Halbert, D. C. Hensley, and M. J. Saltmarsh
Oak Ridge National Laboratory, Oak Ridge, Tennessee 37830

(Received 1 April 1974)

We have measured the excitation function at $\theta_{\text{lab}}=175^\circ$ for the excitation of the first 2^+ state in $^{88}\text{Sr}^*$ by inelastic scattering of ^{22}Ne . At the same time we obtained similar data for the excitation of the first 2^+ state of the beam particle itself. The measurements span the energy range 49–65 MeV containing the region of the Coulomb–nuclear interference. In terms of Rutherford trajectories, the $^{22}\text{Ne}^*$ interference minimum is located at a separation ~ 0.2 fm greater than for $^{88}\text{Sr}^*$. An optical potential was obtained by a fit to elastic scattering data consisting of an excitation function at $\theta_{\text{lab}}=175^\circ$ and an angular distribution at 65.4 MeV lab. A collective model distorted-wave Born-approximation calculation with this potential can account for the $^{88}\text{Sr}^*$ data but fails to describe the shape of the $^{22}\text{Ne}^*$ excitation function.

NUCLEAR REACTIONS $^{88}\text{Sr}(^{22}\text{Ne}, ^{22}\text{Ne})$, $E=49\text{--}65$ MeV; measured $d\sigma(E)$ at $\theta_1=175^\circ$ for g.s., first 2^+ state in ^{88}Sr and ^{22}Ne , $d\sigma(\theta)$ at 65.4 MeV for g.s.; deduced optical model potential, deformation parameters. Enriched target.

I. INTRODUCTION

The interference between Coulomb and nuclear excitation in inelastic scattering with heavy-ion beams¹ possesses several interesting aspects. The pronounced interference structure appearing in the inelastic cross section (as compared with the somewhat featureless structure of elastic scattering) offers the hope that such structure will be useful in resolving ambiguities in the heavy-ion optical potential. Furthermore, the interference minimum is localized far out on the nuclear surface, approximately 2.5 fm beyond the conventional nuclear touching distance $=1.25(A_1^{1/3} + A_2^{1/3})$ fm, where A_1 is the target mass and A_2 is the projectile mass.^{1,2} It is in the region of the interference that the real part of the ion-ion optical potential seems most sensitively determined by the measurements.³ As probed by ^{16}O ions incident on ^{58}Ni , ^{88}Sr , and ^{142}Nd targets the interference minimum is of the order of 1 fm full width.³ It is therefore of interest to examine this structure with an even heavier projectile (i.e. smaller de Broglie wave length).

We have explored this interference phenomenon with ^{22}Ne ions incident on a ^{88}Sr target. We have also observed the Coulomb–nuclear interference in the inelastic excitation of the beam projectile itself. The measurements consist of elastic and inelastic excitation functions at 175° lab from 49 to 65 MeV lab. To facilitate a distorted-wave Born-approximation (DWBA) analysis of the inelastic data, we have measured the elastic scattering angular distribution at 65.4 MeV lab. A

global analysis of the elastic data provided the optical model parameters needed to describe the distorted waves in the incident and exit channels.

II. EXPERIMENTAL METHOD

The excitation function data and the 65.4-MeV angular distribution were obtained in two separate runs with the same scattering chamber. All of the detectors were Si surface-barrier counters. A calibrated α source placed at the target position was used to determine the solid angles of all detectors.

The excitation function at 175° lab was obtained with a 300-mm² annular detector subtending a solid angle of 34 msr. The average angle, weighted according to $\sin\theta$, was actually 175.5° (176.6° c.m.). The angular distribution was obtained with two movable counters which could be positioned to within 0.2° . One counter covered the angles from 65 to 110° with a polar-angle acceptance of $\pm 0.57^\circ$. The other counter, with a polar angle of $\pm 1.14^\circ$ was used for lab angles from 71 to 150° . A monitor counter was fixed at 45° lab, where $^{22}\text{Ne} + ^{88}\text{Sr}$ elastic scattering should follow the Rutherford law over the energy range of interest here.

The Oak Ridge Isochronous Cyclotron (ORIC) accelerated the ^{22}Ne in either its 4^+ or 5^+ charge state. The ion source, of the Penning cold-cathode type,⁴ was operated with natural neon (9.2% ^{22}Ne). Beam currents extracted from the cyclotron were on the order of several hundred nA. The beam was transmitted nondispersively to the scattering chamber by a focus halfway through a bending

magnet.⁵ A phosphorescent screen was placed in the magnet to check the position and focus of the beam spot, after which it was replaced by a small circular aperture to discard stray particles. The annular detector was protected by a tantalum tube of inside diameter 3.5 mm through which the beam passed on its way to the target. With this arrangement, the beam intensity at the chamber entrance was often as high as 40% of that extracted from the cyclotron, and 90% of this passed through the Ta tube. The maximum ^{22}Ne intensity measured in the Faraday cup (after stripping by the target) was about 200 nA.

The beam energies were measured in a calibrated bending magnet. However, we found evi-

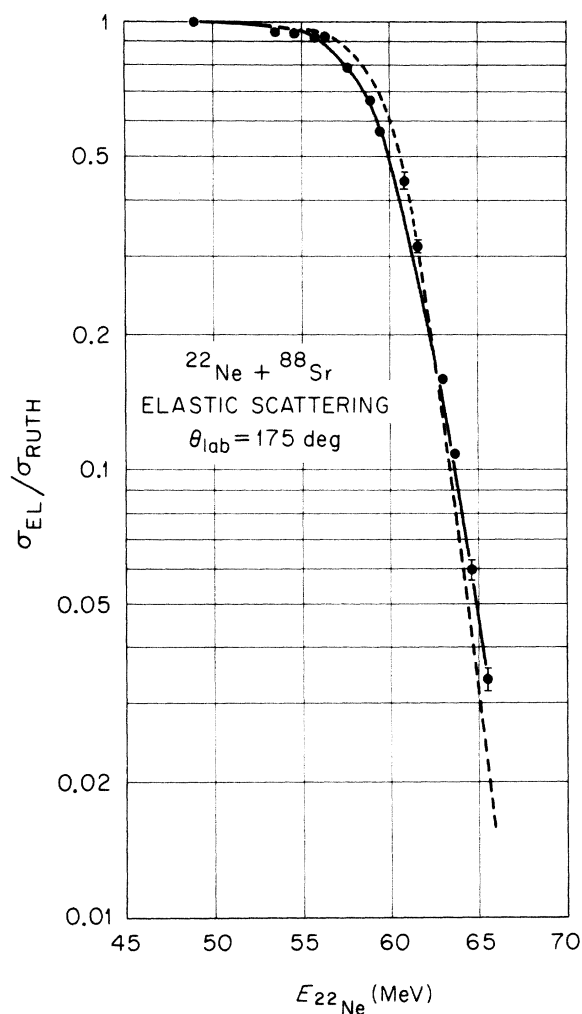


FIG. 1. Elastic scattering excitation function at 175° lab for $^{22}\text{Ne} + ^{88}\text{Sr}$. The data are represented by points with typical error bars. The dashed curve is an optical model calculation using the parameters *NB5* in Table I. The solid curve is an optical model calculation using the parameter set *OR1* of Table I.

dence that the energy on target could drift by 0.1 to 0.4 MeV, due to tune-up of the cyclotron. Corrections determined from the pulse height of the elastic peak were applied to the data. The final energy assignments are accurate to about ± 0.1 MeV. The energy spread of the beam as determined by the calibrated magnet is typically about 0.4% full width at half-maximum (FWHM) (200–300 keV). This spread eliminated ^{20}Ne (1st excited state at 1.63 MeV) from consideration as the beam particle but permitted adequate separation of the 1st excited states of ^{22}Ne and ^{88}Sr .

Four targets ($20\text{--}60 \mu\text{g}/\text{cm}^2$) were prepared by vacuum evaporation of ^{88}Sr onto $20 \mu\text{g}/\text{cm}^2$ carbon backings. The starting material was the carbonate, isotopically enriched to 99.84% in ^{88}Sr , mixed with Ta powder. The targets were transferred in vacuum to the scattering chamber by means of a portable chamber and vacuum lock.

In heavy-ion bombardments large numbers of low-energy electrons are liberated from the target. These must be suppressed for proper operation of surface-barrier detectors. Biasing the target at +350 V (or -350 V) seemed to have no effect. A large permanent magnet was placed outside the chamber and proved adequate except for the annular detector. A thin gold foil stretched in front of the annular counter eliminated this problem. The magnetic deflection of the particles

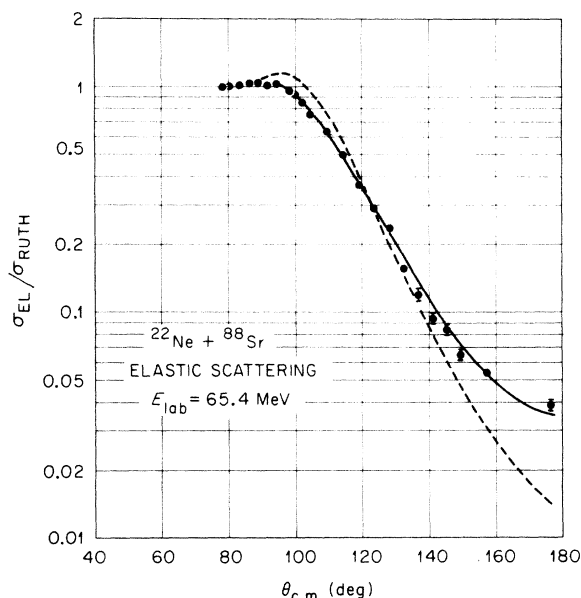


FIG. 2. Elastic angular distribution for $^{22}\text{Ne} + ^{88}\text{Sr}$ scattering at 65.4 MeV. The data are shown as points with typical error bars. The dashed curve is an optical model prediction for the parameter set *NB5* of Table I and the solid curve is the prediction for parameter set *OR1* of Table I.

under study was estimated to be $\sim 0.1^\circ$ and was not considered further.

III. EXPERIMENTAL RESULTS

The spectra were analyzed with a least-squares peak fitting program. The absolute cross sections were calculated from the known Rutherford cross sections for scattering into the monitor and the measured solid-angle ratios. The elastic data are shown in Figs. 1 and 2 and the inelastic data are shown in Fig. 3.

In comparing these data to the data on inelastic excitation of $^{88}\text{Sr}^*$ (1.84 MeV) by ^{16}O beams,³ several comments may be made. The shape of the inelastic excitation function at 175° lab appears to be the same for ^{22}Ne and ^{16}O beams. Referring to the distance of closest approach scale at the top of Fig. 3, the interference minimum is located at

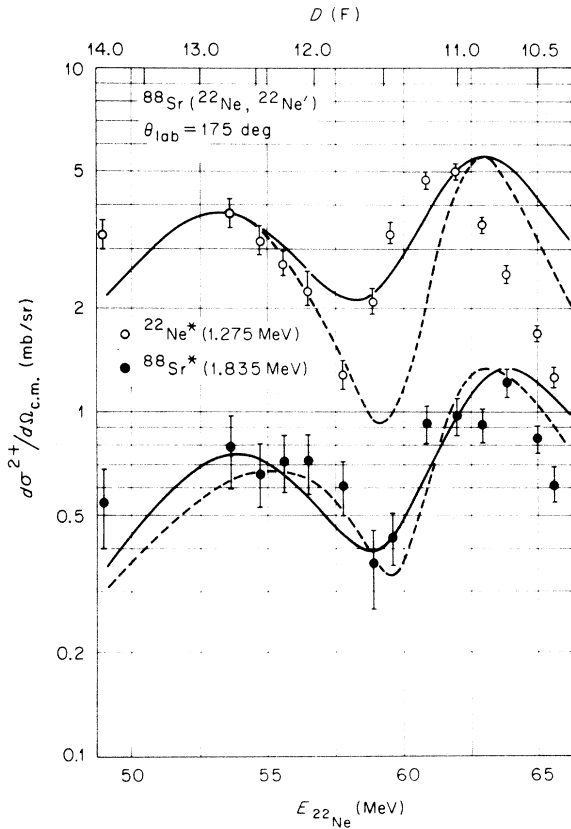


FIG. 3. Inelastic scattering excitation functions at 175° lab for the first 2^+ states in ^{88}Sr (lower figure) and ^{22}Ne (upper figure). The data are shown as points with error bars. The curves are DWBA collective model predictions. The dashed curve is a calculation based on the parameter set NB 5 of Table I whereas the solid curve is based on the parameter set OR1 of Table I. The scale at the top represents distance of closest approach calculated assuming Rutherford trajectories.

11.6 fm. This is 2.5 fm greater than the nuclear touching distance $1.25(A_1^{1/3} + A_2^{1/3})$ fm. The same value of 2.5 fm can be extracted from the 175° $^{16}\text{O} + ^{88}\text{Sr}$ data.³ In comparing elastic scattering angular distributions, it is evident that the rise above Rutherford is much less pronounced for ^{22}Ne on ^{88}Sr (Fig. 1) than for ^{16}O on ^{88}Sr (Ref. 3, Figs. 15 and 16). Finally, it should be pointed out that the interference minimum for excitation of the beam projectile (upper part of Fig. 3) is shifted to a larger distance of closest approach by about 0.2 fm relative to the minimum for ^{88}Sr . A similar effect has been reported for the excitation of ^7Li and ^{18}O beam projectiles.⁶

IV. ANALYSIS AND DISCUSSION

We analyze these data in terms of the collective-model generalization of the DWBA method.⁷ The main attraction of this method is that the form factor is simply related to the derivative of the optical potential used to generate the distorted waves. If the method is applicable, then structure in the inelastic process may provide useful information on the optical parameters.

As we wish to compare our results on $^{22}\text{Ne} + ^{88}\text{Sr}$ inelastic scattering with those for $^{16}\text{O} + ^{88}\text{Sr}$ inelastic scattering,³ we use the same Woods-Saxon shape prescription as used in the analysis of the $^{16}\text{O} + ^{88}\text{Sr}$ data.³ Briefly summarized, the optical potential $V_{\text{opt}}(r)$ is assumed to consist of a Coulomb part, $V_C(r)$, a real nuclear potential, $Vf(r)$, and an imaginary volume absorptive potential $Wg(r)$:

$$V_{\text{opt}}(r) = V_C(r) - Vf(r) - iWg(r), \quad (1)$$

where

$$f(r) = \left[1 + \exp\left(\frac{r - R_0}{a}\right) \right]^{-1}, \quad R_0 = r_0(A_1^{1/3} + A_2^{1/3}), \quad (2)$$

$$g(r) = \left[1 + \exp\left(\frac{r - R'_0}{a}\right) \right]^{-1}, \quad R'_0 = r'_0(A_1^{1/3} + A_2^{1/3}), \quad (3)$$

$$V_C(r) = \begin{cases} Z_1 Z_2 \frac{e^2}{r} & \text{for } r > R_C \\ Z_1 Z_2 \left[3 - \left(\frac{r}{R_C}\right)^2 \right] & \text{for } r < R_C, \\ R_C = 1.25 A_2^{1/3}, \end{cases} \quad (4)$$

and Z_1 , Z_2 are the charges of the projectile and target, respectively.

For quadrupole excitation we use the following matrix element⁷:

$$M_m = \left[\beta \alpha R_0 V \frac{df(r)}{dr} + i \beta' \alpha R'_0 W \frac{dg(r)}{dr} + \frac{3}{5} \beta_C Z_1 Z_2 \frac{(eR_C)^2}{r^3} \right] Y_{2m}, \quad (5)$$

where $\alpha = A_2^{1/3}/(A_1^{1/3} + A_2^{1/3})$ and β , β' , and β_C are deformation parameters for the real nuclear potential, the absorptive nuclear potential, and the Coulomb potential, respectively. The transition amplitude for inelastic scattering from an initial state i to a final state f is then given by⁷:

$$T_{if} = \int d\vec{r} \phi_f^{(-)*}(\vec{k}_f, \vec{r}) M \phi_i^{(+)}(\vec{k}_i, \vec{r}), \quad (6)$$

where the ϕ 's are distorted waves describing the relative motion of the $^{22}\text{Ne} + ^{88}\text{Sr}$ system for relative momentum \vec{k} . In the spirit of the DWBA method, ϕ is the solution of the Schrödinger equation for the potential given by Eq. (1) where the parameters V , W , r_0 , r'_0 , a , and a' are determined from a least-squares fit to the elastic scattering data.

To obtain optical model parameters which describe the measured $^{22}\text{Ne} + ^{88}\text{Sr}$ elastic scattering (Figs. 1 and 2) we started with a set of parameters which accounted for $^{16}\text{O} + ^{88}\text{Sr}$ elastic scattering.⁸ The predictions of this parameter set, labeled *NB5* in Table I, are shown as the dotted curves in Figs. 1 and 2. In all the calculations discussed herein, we have used 75 partial waves and radial integration steps of 0.2 fm out to 100 fm. These conditions were shown to be adequate by subsidiary calculations. Alterations were made to the optical model search program GENOA⁹ and the DWBA program DWUCK¹⁰ to accommodate this many partial waves and radial integration steps. Keeping r_0 fixed at 1.3 fm, we searched on V , W , r'_0 , a , and a' . With relatively minor changes, except in W , we obtained the improved fit to elastic scattering shown as the solid curves in Figs. 1 and 2. The parameters are shown in Table I as parameter set *OR1*.

The collective-model results for the inelastic scattering with these potentials are shown in Fig. 3. The Coulomb and nuclear deformation parameters were adjusted to obtain the best fits to the data. The deformation lengths used to fit our ^{88}Sr data were $\beta_C r_C A_2^{1/3} = 0.69$ fm for the Coulomb amplitude, $\beta r_0 A_2^{1/3} = 0.46$ fm for the real nuclear amplitude, and $\beta r' A_2^{1/3} = 0.50$ fm for the imaginary nuclear amplitudes. These can be compared with the values found in an analysis³ of ^{16}O inelastic scattering from ^{88}Sr where corresponding values of 0.70, 0.64, and 0.64 fm were obtained. Deformation parameters for ^{88}Sr obtained by ^{16}O and

TABLE II. Comparison of ^{88}Sr deformation parameters obtained by ^{16}O inelastic scattering (Ref. 3) and by ^{22}Ne inelastic scattering.

Projectile	β_C	β	β'
^{16}O	0.124	0.11	0.10
^{22}Ne	0.126	0.08	0.08

^{22}Ne inelastic scattering are also compared in Table II. The Coulomb deformation amplitudes are in excellent agreement as are the locations of the interference minima relative to the nuclear touching distance. However, the nuclear deformation amplitude for ^{88}Sr extracted from ^{22}Ne inelastic scattering data appears to be significantly smaller than that obtained by an analysis of ^{16}O inelastic scattering. We also note that, in both experiments, the nuclear deformation parameters required to fit the data are definitely smaller than the Coulomb deformation parameters even though a consistent analysis method has been used for the entire excitation function. Although the two parameter sets in Table I give very different predictions for elastic scattering (Figs. 1 and 2), they both give a reasonable account of the inelastic scattering (lower part of Fig. 3). This success of the DWBA collective model in accounting for inelastic excitation of $^{88}\text{Sr}^*$ by ^{22}Ne beams confirms the applicability of the method to heavy-ion inelastic scattering previously established for ^{16}O beams^{3, 11} and ^{11}B beams.¹²

In contrast, the excitation function for the first 2^+ state in ^{22}Ne (the upper part of Fig. 3) cannot be adequately accounted for by the direct-reaction collective model used here. Deformation parameters $\beta_C = 0.40$ and $\beta = 0.28$ were used to match the relative magnitudes of the two bumps in the inelastic excitation function but then the general shape is not well reproduced. If changes in the deformation parameters are made to improve the shape and location of the interference minimum, then the relative magnitudes of the two bumps are no longer well accounted for. The fits to these data represent a clear failure of the collective model DWBA method and a coupled-channels or other multi-step approach is apparently needed.

TABLE I. Optical model parameters.

	V (MeV)	r_0 (fm)	a (fm)	W (MeV)	r' (fm)	a' (fm)
<i>NB5</i>	23.73	1.3	0.568	3.30	1.4	0.323
<i>OR1</i>	21.54	1.3	0.56	9.54	1.4	0.36

ACKNOWLEDGMENTS

It is a pleasure to acknowledge a stimulating correspondence with F. Videbaek concerning the analysis of these data. We are indebted to L. Owens for the necessary adjustments to the programs GENOA⁹ and DWUCK¹⁰ so that they can be

used to analyze heavy-ion data. We extend our thanks to M. B. Marshall and the ORIC operations staff for successful operation of the cyclotron. The excellent α source prepared by C. E. Bemis

facilitated solid angle calibrations. Finally, we wish to recognize the contributions of E. D. Hudson, R. S. Lord, and M. L. Mallory in extending the ORIC capabilities to the heavy-ion regime.

†Research supported by the U. S. Atomic Energy Commission under contract with Union Carbide Corporation.

¹F. Videbaek, I. Chernov, P. R. Christensen, and E. E. Gross, *Phys. Rev. Lett.* **28**, 1072 (1972).

²J. A. Thomson, R. P. Scharenburg, and R. W. Lutz, *Phys. Rev.* **14**, 1699 (1971).

³P. R. Christensen, I. Chernov, E. E. Gross, R. Stokstad, and F. Videbaek, *Nucl. Phys.* **A207**, 433 (1973).

⁴M. L. Mallory, E. D. Hudson, and G. Fuchs, *IEEE Trans. Nucl. Sci.* **NS-19**, 118 (1972).

⁵J. E. Draper, *Rev. Sci. Instrum.* **37**, 969 (1966).

⁶K. Katori, C. L. Fink, G. C. Morrison, J. L. Yntema, and B. Zeidman, Argonne National Laboratory Report

No. PHY-1973B, 1973 (unpublished), p. 557.

⁷R. H. Bassel, G. R. Satchler, R. M. Drisko, and E. Rost, *Phys. Rev.* **128**, 2693 (1962).

⁸F. Videbaek, K. Ulbak, O. Hansen, and P. R. Christensen, Argonne National Laboratory Informal Report No. PHY-1973B, 1973 (unpublished), p. 663.

⁹F. G. Perey, private communication.

¹⁰P. D. Kunz, private communication.

¹¹F. D. Becchetti, D. G. Kovar, B. G. Harvey, J. Mahoney, B. Mayer, and F. G. Pülhofer, *Phys. Rev.* **C 6**, 2215 (1972).

¹²J. L. C. Ford, K. S. Toth, D. C. Hensley, R. M. Gaedke, P. J. Riley, and S. T. Thornton, *Phys. Rev.* **C 8**, 1912 (1973).